Journal of Applied Polymer Science

Enhancement of interlaminar fracture toughness of carbon fiber–epoxy composites using polyamide-6,6 electrospun nanofibers

Bertan Beylergil,[1] **Metin Tanoğlu**,[1] **Engin Aktaş**[2]
[1]Faculty of Engineering, Department of Mechanical Engineering, Izmir Institute of Technology, Urla Izmir 35340, Turkey
[2]Faculty of Engineering, Department of Civil Engineering, Izmir Institute of Technology, Urla Izmir 35340, Turkey
Correspondence to: M. Tanoğlu (E-mail: metintanoglu@iyte.edu.tr)

ABSTRACT: In this study, carbon fiber–epoxy composites are interleaved with electrospun polyamide-6,6 (PA 66) nanofibers to improve their Mode-I fracture toughness. These nanofibers are directly deposited onto carbon fabrics before composite manufacturing via vacuum infusion. Three-point bending, tensile, compression, interlaminar shear strength, Charpy impact, and double cantilever beam tests are performed on the reference and PA 66 interleaved specimens to evaluate the effects of PA 66 nanofibers on the mechanical properties of composites. To investigate the effect of nanofiber areal weight density (AWD), nanointerlayers with various AWD are prepared by changing the electrospinning duration. It is found that the electrospun PA 66 nanofibers are very effective in improving Mode-I toughness and impact resistance, compressive strength, flexural modulus, and strength of the composites. However, these nanofibers cause a decrease in the tensile strength of the composites. The glass-transition temperature of the composites is not affected by the addition of PA 66 nanofibers. © 2017 Wiley Periodicals, Inc. J. Appl. Polym. Sci. **2017**, *134*, 45244.

KEYWORDS: composites; electrospinning; mechanical properties; polyamides

Received 18 January 2017; accepted 21 April 2017
DOI: 10.1002/app.45244

INTRODUCTION

Laminated composites have been extensively used in many structural applications because of their high strength and stiffness at low weight and good corrosion-resistance and fatigue properties. However, they are prone to delamination damage, which may occur for a variety of reasons, such as low-velocity impact events, manufacturing imperfections, and stress concentrations triggered by sudden changes in structural details.[1,2] Delamination may cause loss of support of the load-bearing layers, which results in accelerated growth of damage and premature failure. Moreover, laminated composites become more vulnerable to environmental influences such as moisture or contaminant penetration because of this type of failure.[1,2] Therefore, researchers have focused on improving the delamination resistance of these composites. What are called $2^1/_2$D composite materials, such as through-thickness stitched or pinned composites, have been developed by some researchers. Over the past decade, there have also been considerable developments in three-dimensional (3D) woven composites made by weaving, braiding, and knitting. These developments were shown to be very successful in improving the damage tolerance of fiber-reinforced composites. However, it was proved that these modifications resulted in a significant reduction in the in-plane mechanical properties of these composites.[3] Steeves and Fleck[4] showed that the presence of z-pins decreases the tensile and compressive strength of the composites by 27% and 30%, respectively. Reeder[5] revealed an about 30% reduction in the tensile strength of the composites due to fiber misalignments caused by the stitching operation. It was also found that the in-plane tension, compression, and flexural properties of the 3D composite are 10 to 40% lower than those for the 2D composites.[6–9] In addition, these techniques do not hinder the initiation of damage; they only enhance the resistance to crack growth once the damage has been initiated.

An alternative technique to improve fracture toughness, the incorporation of micro- or nanofillers into the matrix phase, has also been studied in recent years. It is well known that this approach has some disadvantages, such as the difficulty of dispersing micro- or nanofillers into the epoxy matrix and the enormously increased resin viscosity that is due to these fillers. The latter especially is a critical problem for out-of-autoclave composite manufacturing techniques such as resin transfer molding and vacuum infusion. An interleaving technique, based on the insertion of a thermoplastic or thermoset material in the interlaminar region, has been developed by some researchers.[10–14] Various interleaf materials such as thermoplastic and thermoset films, nonwoven veils, and self-same resin interleaf materials have been studied. Saz-Orozco *et al.*[15] investigated the

effects of a polyamide (PA) veil on the interlaminar fracture toughness of a glass fiber–vinyl ester composite. With the addition of the PA veil, the Mode-I interlaminar fracture toughness values at crack initiation and propagation were found to be improved by 59% and 90%, respectively. However, the PA veils composed of microfibers resulted in an unavoidable compromise in in-plane mechanical properties such as tensile and flexural properties at the expense of reduced carbon fiber volume fraction and increased thickness.

Recently, the use of electrospun thermoplastic nanofibers has emerged as a promising technique to toughen laminated composites without deteriorating the in-plane mechanical properties. Although this approach requires an extra step in the manufacturing of composite laminates, there is no need for a radical change in the processing route. Therefore, it can be easily adapted to traditional composite manufacturing techniques. Van der Heijden *et al.*[16] improved the interlaminar fracture toughness of infusion-molded laminates by using electrospun poly-e-caprolactone nanofibers. Herwan *et al.*[17] proved that the load-bearing capacity of pin-joined composite laminates can be improved by introducing polyacrylonitrile (PAN) nanofibers between dry carbon fabrics. Bilge *et al.*[18] investigated the effects of polystyrene-*co*-glycidyl methacrylate [P(St-*co*-GMA)] nanofibers on carbon fiber–epoxy composites subjected to in-plane loading. They concluded that P(St-*co*-GMA) nanofibers were moderately efficient in improving the in-plane properties of carbon fiber–epoxy composites. Most of the studies in the literature focused on the polyamide-6,6 (PA 66) nanofiber interleaving system because PA 66 polymer has many advantages over other classes of engineering polymers, such as high melting temperature, superior fiber-forming ability, good compatibility with uncured resin, and good mechanical properties.[19] Daelemans *et al.*[20] used PA 66 and PA 69 nanofibers to improve the fracture toughness of carbon fiber–epoxy composites. They showed that these nanofibers could increase the Mode-I fracture toughness about 28% and 42%, respectively. The main mechanism for improving toughness values was the bridging of microcracks within the composite by the PA nanofibers. Another study by Daelemans *et al.*[21] showed that randomly oriented nanofibers are more effective than aligned nanofibers for improving the fracture toughness of carbon fiber–epoxy (CF/EP) composites. A recent study by Brugo and Palazzetti[22] revealed that the architecture of the fabric (unidirectional (UD) or woven) and the thickness of the nanointerlayer were significant parameters in improving the delamination resistance of composites. The transition of the nanofiber-interleaving technique into commercial products has already started, and now the first commercial supplies of thermoplastic nanoveils are on the market. However, there is a lack of research on this subject, and it has to be enlarged for wider acceptance of these materials in composite industry. There is no published work investigating the effects of PA 66 electrospun nanoveils on the mechanical behavior of CF/EP composites manufactured by the vacuum-infusion technique. Additionally, there is no report in the literature on the tensile and compressive properties of carbon fiber–epoxy composites interleaved with electrospun PA 66 nanofibers. This study aims to make a unique contribution in this research gap and develop a better understanding of the effects of PA 66 nanofibers on the mechanical performance of existing CF/EP composites.

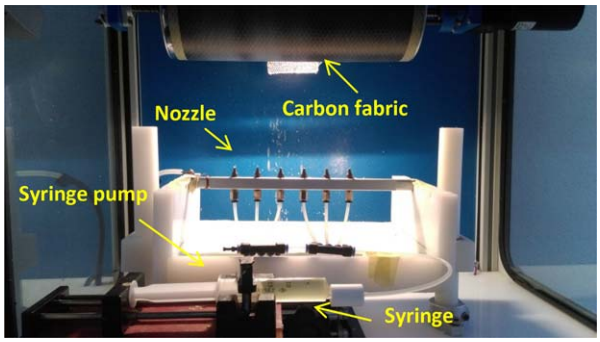

Figure 1. Photograph of the electrospinning system currently used in our laboratory. [Color figure can be viewed at wileyonlinelibrary.com]

In this study, reference and PA 66 interleaved unidirectional CF/EP composite laminates were manufactured by the vacuum-infusion technique. A series of mechanical tests, specifically three-point bending, tensile, compression, interlaminar shear strength (ILSS), Charpy impact, and double cantilever beam (DCB), were performed on prepared specimens to investigate the effects of PA 66 nanofibers on the mechanical performance of CF/EP composites. The thermomechanical behavior of the composites was also investigated by dynamic mechanical analysis (DMA). The results showed that the Mode-I fracture toughness of CF/EP composites can be increased about 50% by using only 1 gsm (gram per square meter) of PA 66 nanofibers at the interface of the carbon fabric and the epoxy matrix. Although incorporation of the nanofibers resulted in a reduction in tensile strength values, these nanofibers could enhance the flexural and compressive properties of the composites with an insignificant weight and thickness increase. Another important observation was that Charpy impact strength of the composites was increased with the incorporation of these nanofibers in the interlaminar region. The DMA results indicated that the glass-transition temperature (T_g) of the composites was not affected by the addition of PA 66 nanofibers. Unlike the other toughening methods, this "win–win" situation is the unique characteristic of the thermoplastic nanofiber interleaving technique.

EXPERIMENTAL

Materials

Unidirectional carbon fabrics with a unit weight of 350 g/m^2 were used as reinforcement material. The epoxy resin (Momentive L160, Hexion Inc., Columbus, Ohio) and its hardener (Momentive H160, Hexion Inc., Columbus, Ohio) were used with the weight ratio of 80:20, respectively. Polyamide-6,6 (PA 66) pellets, formic acid, and chloroform were used for the preparation of the polymer solution for electrospinning.

Preparation of PA 66 Nanofibers

PA 66 nanofibers were produced by the electrospinning process using the electrospinning setup in our laboratory shown in Figure 1. It consists of six nozzles that provide larger, uniform nanofibrous nonwovens, a cylindrical translating–rotating

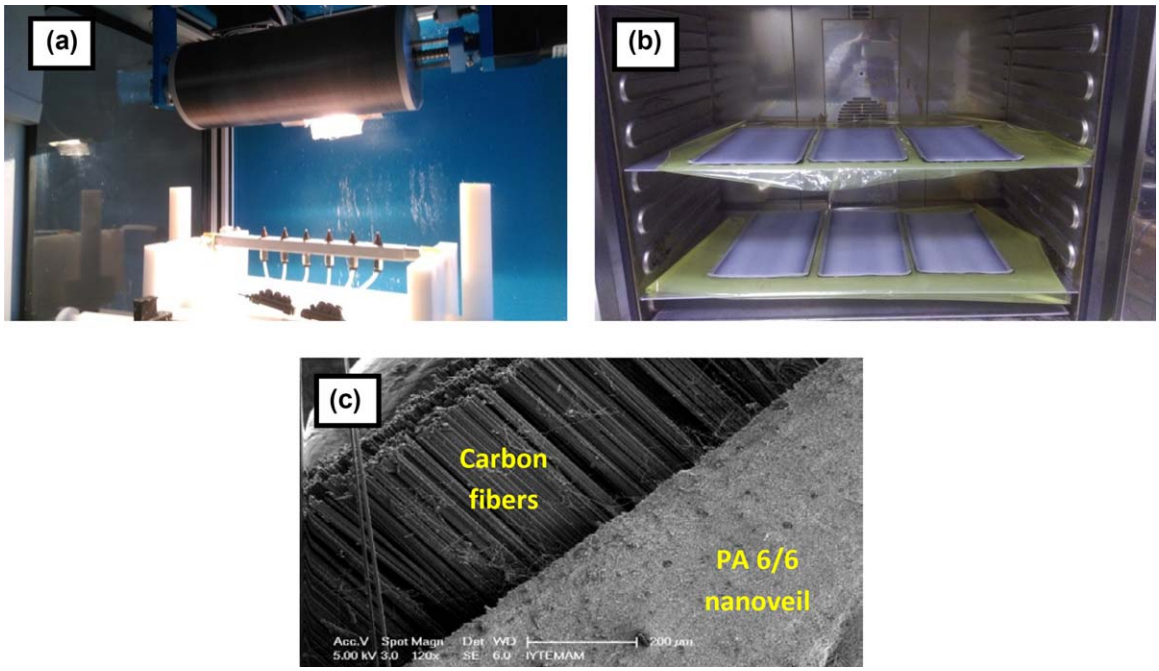

Figure 2. (a) Deposition of PA 66 nanofibers, (b) unidirectional carbon fabrics after PA 66 nanofiber deposition, and (c) SEM image of PA 66 nanoveil deposited on carbon fabric. [Color figure can be viewed at wileyonlinelibrary.com]

collector, and a syringe pump. To produce PA 66 nanofibers, a 10 wt % PA 66 solution was prepared by dissolving 10 g of PA 66 pellets in 100 mL of formic acid/chloroform (75:25 v/v) at room temperature. This specific concentration was selected to prepare the PA 66 nanofibers with the optimum properties as suggested by Sanatgar *et al.*[23]

Deposition of PA 66 Nanofibers on Carbon Fabrics

The prepared solution was loaded into a 20 mL syringe that is attached to a syringe pump. The flow rate of the PA 66 solution was adjusted to 6 mL/h (1.0 mL/h for each nozzle), and the applied voltage and the tip-to-collector distance were kept as 30 kV and 12 cm, respectively. These working parameters were selected to produce uniform and bead-free PA 66 nanofibers based on our experience and the recommendation by Matulevicius *et al.*[19] The electrospinning duration was adjusted to 30 and 60 min in order to investigate the effects of nanofiber areal weight density.

Figure 2(a) shows the deposition of PA 66 nanofibers onto unidirectional carbon fabrics. To remove residual solvents, the carbon fabrics with PA 66 nanofibers were kept at 60 °C for 3 h [Figure 2(b)] before vacuum infusion. In order to determine the areal density of the nonwoven fabric, two additional carbon fabrics were coated with PA 66 nanofibers for 30 and 60 min. Then the nanofibrous veil was carefully peeled off from the surface of the carbon fabric and cut into small pieces. They were weighed with an accuracy of 0.0001 g. The average nanofiber areal weight density (AWD) values for 30 and 60 min of deposition were determined approximately as 0.525 g/m^2 and 1.05 g/m^2, respectively. This corresponds to a 0.15% and 0.30% weight increase of the carbon fabric, which is insignificant for those fabrics (350 g /m^2 areal density).

Differential scanning calorimetry (DSC) was used to determine the thermal properties of the electrospun PA 66 mat. The sample of the mat taken from the surface of the carbon fabric was heated from room temperature to 350 °C at a heating rate of 10 °C/min under a nitrogen atmosphere. Figure 3 shows the DSC curve of the PA 66 nanofiber mat. The melting temperature (T_m) and T_g of the PA 66 nanofiber mat were determined as 256.2 °C and 48.80 °C, respectively. These results are consistent with that obtained by Goodarz *et al.*[24] As will be shown in later sections, the PA 66 nanofibers will retain their morphology in the final composite laminates because the curing temperature of the epoxy is well below the melting temperature of the PA 66 nanofiber mat.

Manufacturing of Composite Test Specimens

The reference and PA 66–modified composites with four layers of unidirectional carbon fabrics were fabricated by the vacuum-infusion

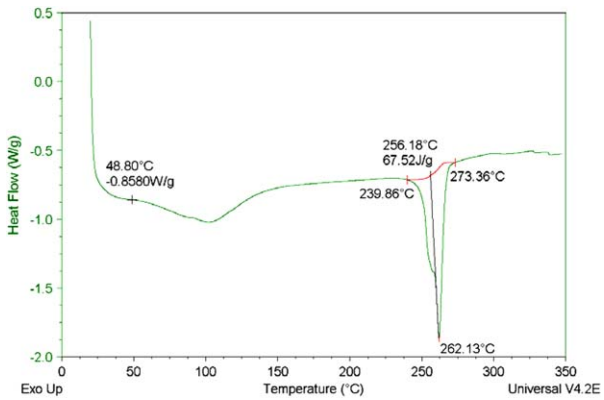

Figure 3. DSC curve of the PA 66 nanofiber mat. [Color figure can be viewed at wileyonlinelibrary.com]

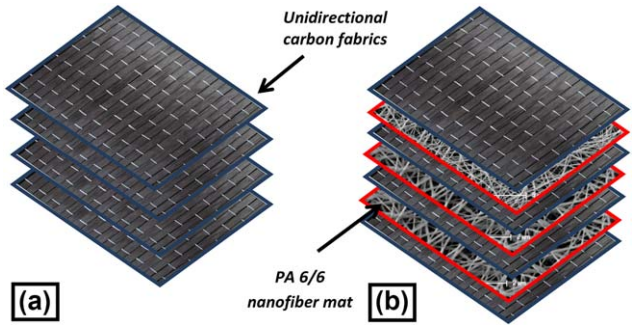

Figure 4. Schematic representation of the (a) reference and (b) interleaved composite laminates. [Color figure can be viewed at wileyonlinelibrary.com]

technique. A polyimide film (Kapton, 50 μm thick) was inserted in the middle of the plies to form an initial crack along the interlaminar region of the DCB specimens. Based on the visual observations during the vacuum-infusion process, no change of the resin flow due to the nanofibers was detected. Demolding of the manufactured composites was carried out after complete curing at room temperature, followed by a postcuring in an oven at 80 °C for 12 h. The fabricated composites were cut into the desired dimensions using a water-cooled diamond saw. The cut edges of the specimens were lightly sanded with 280 grit sandpaper by hand. The thickness of the specimens (h) was measured to be in the range of 1.23–1.26 mm. The effect of PA 66 nanofibers on the final thickness of the specimen was less than 2%. No additional weight gain was observed due to nanofiber interleaving. Figure 4 is a schematic representation of the reference and interleaved composite laminates. The fiber volume fraction (V_f) of the specimens was determined by the Archimedes principle; V_f varied in the range of 0.54–0.55 for all specimens. No significant change was observed in V_f after the addition of PA 66 nanofibers.

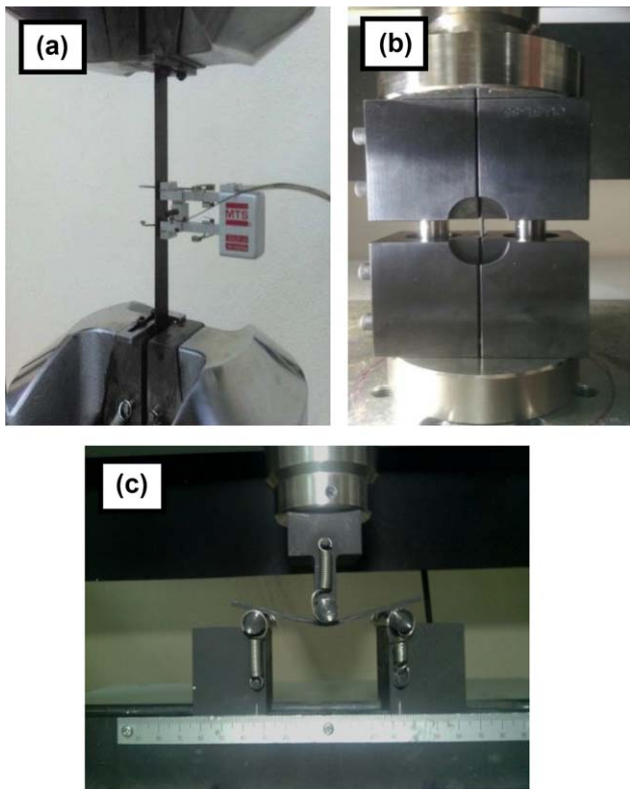

Figure 5. Photographs of the test specimens under (a) tensile and (b) compressive loading and (c) three-point bending. [Color figure can be viewed at wileyonlinelibrary.com]

Mechanical Testing

All mechanical tests were performed at ambient conditions in accordance with the relevant ASTM standards.[25–28] Tensile tests were carried out at a constant crosshead speed of 2.0 mm/min up to failure. The dimensions of the test specimens were 250 mm in length and 15 mm in width. A clip-on extensometer with knife edges was used to measure the strain [Figure 5(a)]. The extensometer was removed from the test specimen after sufficient strain data were collected. Then the specimen was tested until failure. Tensile gripping end tabs were attached to the specimen to reduce the stress concentrations in the grip areas. The compressive strength and modulus of the specimens in the longitudinal direction were determined. The dimensions of the compression test specimens were 140 mm in length and 12.7 mm in width. The gauge length was 12.7 mm. The specimens were placed in an antibuckling fixture and loaded until failure at a constant crosshead speed of 2.0 mm/min [Figure 5(b)].

The flexural properties of the reference and PA 66–modified specimens were obtained from three-point bending tests [Figure 5(c)]. The span-to-thickness ratio and test speed were 32:1 and 2.10 mm/min, respectively. Interlaminar shear strength tests were conducted using the short beam shear test. The span-to-thickness ratio and test speed were 6:1 and 1 mm/min, respectively.

The Mode-I interlaminar fracture toughness of the composites was determined by double cantilever beam (DCB) experiments using a Shimadzu AGS-X, Kyoto, Japan, universal test machine fitted with a 5 kN load cell. The dimensions of the DCB test specimens were L = 150 mm in length and b = 25 mm in width. Aluminum blocks were bonded to the outer surfaces of the DCB specimens to transfer the opening forces. The configuration of the specimens for DCB testing is shown in Figure 6. Each specimen was initially loaded with a crosshead speed of 1 mm/min, and the crack was allowed to propagate a short distance (3–5 mm) before the specimen was unloaded. Then the specimen was loaded until the crack propagated about 70 mm from the tip of the crack. Load, opening displacement, and crack length were recorded for the energy release rate (G_I) calculation during the tests. The G_I was calculated using the modified beam theory data-reduction method, as follows[15]:

$$G_I = \frac{F}{N}\frac{3P\delta}{2b(a+|\Delta|)} \quad (1)$$

where G_I is the Mode-I interlaminar fracture toughness, P is the applied load, δ is the load point displacement, b is the specimen width, a is the delamination length (crack length), Δ is a value that is determined experimentally by generating a least-squares plot of the cube root of compliance ($C^{1/3}$) as a function of

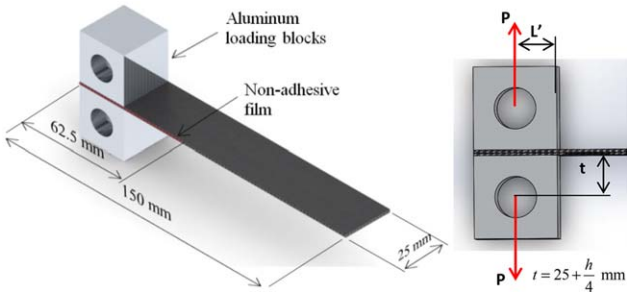

Figure 6. Schematic representation of the DCB test specimens. [Color figure can be viewed at wileyonlinelibrary.com]

delamination length, and F and N are the correction parameters to take into account a large displacement and the stiffening of the specimens by the loading blocks, respectively. These correction factors can be calculated using the following equations[29]:

$$F = 1 - \left(\frac{3}{10}\right)\left(\frac{\delta}{a}\right)^2 - \left(\frac{3}{2}\right)\left(\frac{\delta t}{a^2}\right) \quad (2)$$

$$N = 1 - \left(\frac{L'}{a}\right)^3 - \left(\frac{9}{8}\right)\left[1 - \left(\frac{L'}{a}\right)^2\right]\left(\frac{\delta t}{a^2}\right) - \frac{9}{35}\left(\frac{\delta}{a}\right)^2 \quad (3)$$

where t and L' are shown in Figure 6. The G_{IC} initiation ($G_{IC,ini}$) value was determined as the value of G_{IC} at which the delamination was visually observed on the edge of the specimen. The G_{IC} propagation ($G_{IC,prop}$) value was calculated as the average of the values of G_{IC} during crack propagation.[9] Figure 7 shows a DCB specimen under Mode-I loading.

Charpy impact tests were carried out on the reference and PA 66 nanofiber interleaved specimens according to the ISO-179 standard on 10 × 80 mm rectangular notched specimens, using a CEAST Resil Impactor, Corporate Consulting, Service & Instruments, Inc., Akron, Ohio, having a maximum hammer energy of 15 J and a hammer tangential speed of 3.46 m/s. At least six specimens were tested to determine the Charpy impact strength of the composites. Figure 8 shows the composite test specimens before and after impact loading.

Scanning Electron Microscopy and Dynamic Mechanical Analysis

Scanning electron microscopy (SEM) observations were made to determine nanofiber morphology and to better understand

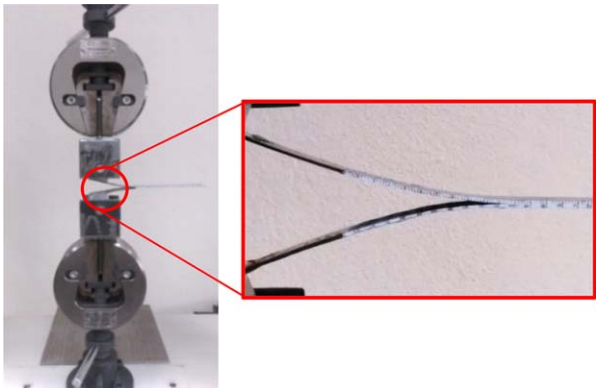

Figure 7. DCB test specimen under Mode-I loading. [Color figure can be viewed at wileyonlinelibrary.com]

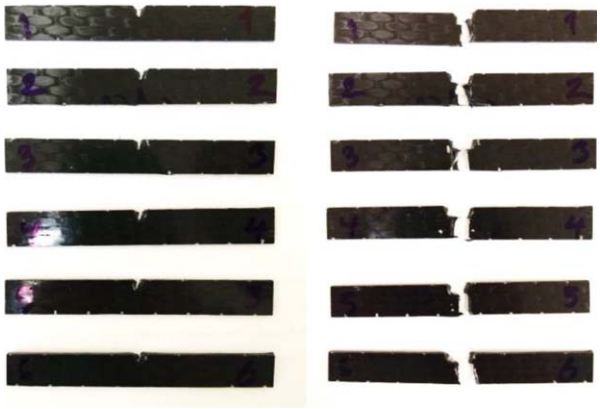

Figure 8. Composite test specimens before and after impact loading. [Color figure can be viewed at wileyonlinelibrary.com]

the failure modes. The specimens were sputter-coated with gold for 90 s and examined under a Philips XL 30S FEG (Eindhoven, The Netherlands) scanning electron microscope. The dynamic mechanical analysis (DMA) was carried out on the specimens using a DMA Q800 (TA Instruments, New Castle, DE) in a dual cantilever mode. The dimensions of the specimens were 65 mm in length and 10 mm in width. At least three specimens were tested for each laminate. The heating rate was 2 °C/min from room temperature to 150 °C, and the frequency was 1 Hz. The storage modulus, loss modulus, and tan δ of the reference and PA 66 nanofiber–modified specimens were determined.

RESULTS AND DISCUSSION

Nanofiber Morphology

Figure 9 shows the SEM images of the electrospun PA 66 nanofibers produced. A continuous and uniform nanofiber network without bead formation was obtained using the selected electrospinning working parameters. The average nanofiber diameter distribution was determined by measuring 50 nanofibers. The average nanofiber diameter was measured as 87 ± 22 nm. It is well known that the nanofiber diameter has a significant effect on the interlaminar fracture toughness of the composites. Therefore, in this study, the diameters of the nanofibers were statistically analyzed by a Weibull distribution at a reliability level of 90%. Figure 10 shows the regression lines and Weibull distribution plot for the probability of nanofiber diameter. The nanofiber diameter was determined as 110 nm.

Mechanical Test Results

Figure 11 shows the representative load-displacement curves of the composite specimens under flexural loading. The load values increased up to a maximum level almost linearly within the elastic region. In the PA 66–modified specimens, failure occurred gradually below this level. The flexural modulus and strength values of the composite specimens in the longitudinal direction are given in Table I. It was observed that the incorporation of PA 66 nanofibers into the interlaminar region results in an improvement of the flexural modulus and strength of the composites. It was found that those values were increased by 15.64% and 12.80% for the composites that contain PA 66 nanofibers with a nanofiber AWD of 1.05 g/m^2. This may be associated with the improved

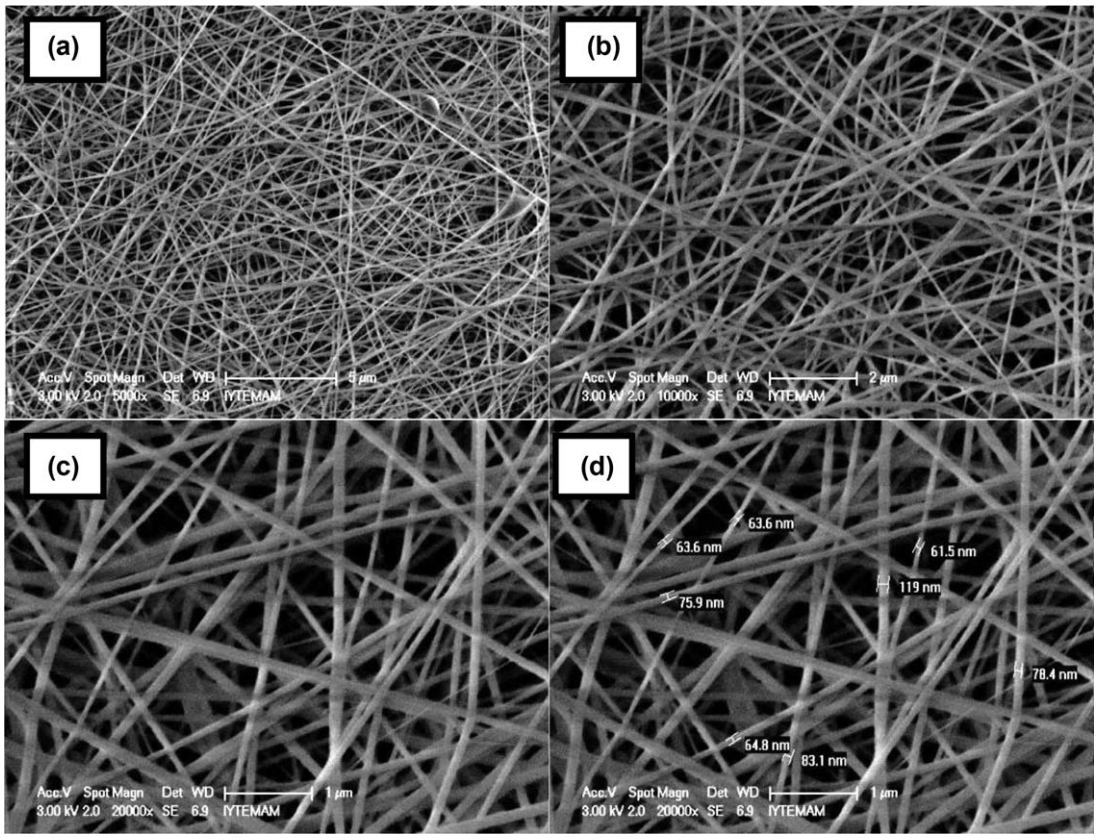

Figure 9. SEM images of PA 66 nanofibers at (a) 5000×, (b) 10,000×, (c) 20,000×, and (d) 20,000 × magnification.

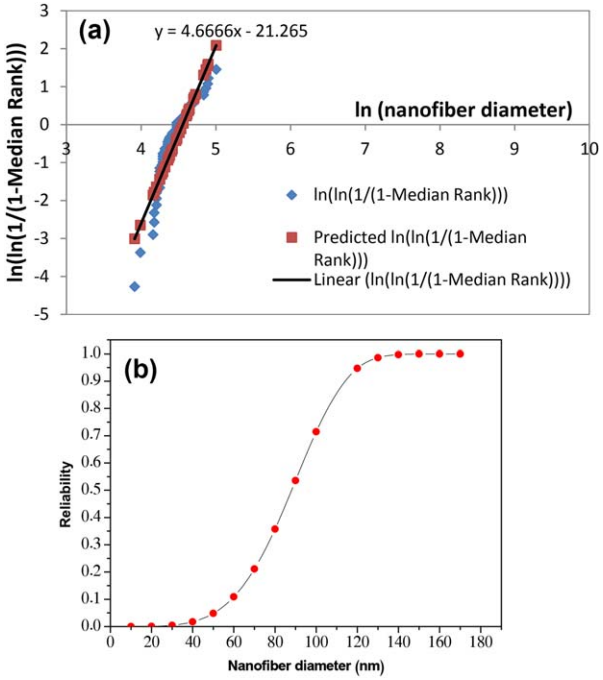

Figure 10. (a) Regression line and (b) Weibull distribution plot for probability of nanofiber diameter. [Color figure can be viewed at wileyonlinelibrary.com]

load-transfer capacity between the carbon fibers that is due to the presence of nanofiber interleaving. Moreover, the modified matrix properties may increase the in-plane bending performance. These findings are consistent with those reported in the literature by Herwan *et al.*[17] and Palazzetti.[30] It was also noteworthy that the flexural properties of the composites increased with the increase of the PA 66 nanofiber AWD value.

The tensile properties of the reference and PA 66–modified test specimens in the longitudinal direction are given in Table I. A

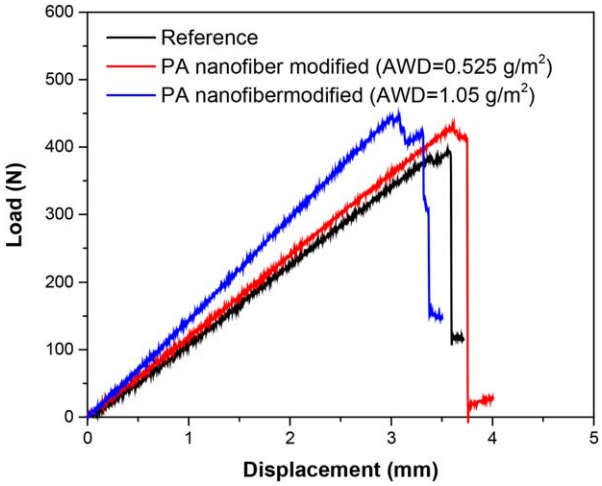

Figure 11. Representative load-displacement curves of the specimens under flexural loading. [Color figure can be viewed at wileyonlinelibrary.com]

Table I. Tensile, Flexural, ILSS, and Charpy Impact Test Results of the Composites with and Without PA 66 Nanofibers

Mechanical property	Reference specimen	PA 66 modified specimens (AWD = 0.525 g/m^2)	PA 66 modified specimens (AWD = 1.05 g/m^2)
Flexural modulus (GPa)	80.1 ± 4.2	90.41 ± 3.3	92.62 ± 2.4
Flexural strength (MPa)	1207.2 ± 49.6	1355.4 ± 67.4	1361.7 ± 116.9
Tensile modulus (GPa)	122.2 ± 3.4	121.5 ± 8.8	120.8 ± 3.93
Ultimate tensile strength (MPa)	1792.4 ± 96	1713.4 ± 195	1616.2 ± 208
ILSS (MPa)	53.3 ± 0.4	55.2 ± 0.4	58.5 ± 0.3
Charpy impact strength (kJ/m^2)	81.4 ± 11.8	87.2 ± 15.0	96.1 ± 6.9

minor decrease (about 1.2%) in tensile modulus was noted for the PA 66 nanomodified specimens. Thus, it was found that the tensile modulus is not significantly affected by the incorporation of these nanofibers. It was also observed that the standard deviations of the tensile strength data of the nanomodified specimens were higher than those of the reference specimens. This may be related to local mat thickness variations in the interlaminar region. PA 66 nanofibers with a nanofiber AWD of 1.05 g/m^2 reduced the tensile strength about 9.8%.

Figure 12 shows the compression test results of both reference and PA 66–modified composite specimens. The values in the parentheses show the standard deviation for the test results. It was found that the compressive strength of the CF/EP composites was increased with the incorporation of PA 66 nanofibers. It was also observed that the compressive strength further increased with increasing PA 66 nanofiber thickness within the interlaminar region. The compressive strength was increased about 15%, due to the presence of nanofibers with an AWD of 1.05 g/m^2. Due to their network structure at the fiber–matrix interphase, a better mechanical attachment together with chemical bonding is expected to occur. This may be associated with improved strength values. As expected, the presence of PA 66 nanofibers within the interlaminar region had no significant effect on the compressive modulus of the specimens. The compressive modulus of the specimens remained unchanged, with values around 100 GPa. This is because the compressive modulus in the longitudinal direction is dominated by the compressive modulus of the carbon fibers. Also, no thickness variation was recorded for the modified specimens.

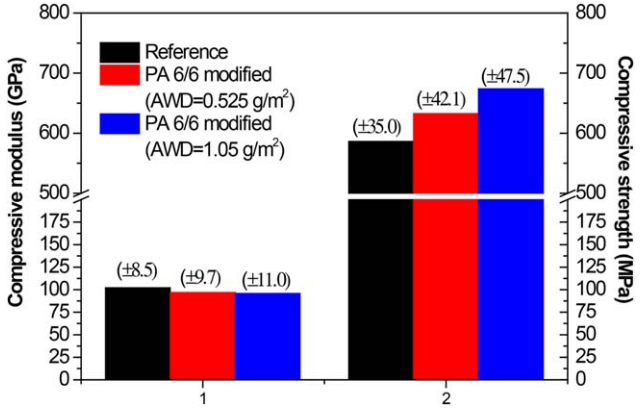

Figure 12. Compression test results of the CF/EP composites. [Color figure can be viewed at wileyonlinelibrary.com]

Table I shows the interlaminar shear properties of the reference and PA 66–modified test specimens. The ILSS of the reference composites was found to be about 53 MPa, due to the presence of PA 66 nanofibers with AWD of 1.05 g/m^2; the ILSS values could be increased by up to 9.65%. This can be associated with the prevention of stress concentrations and crack initiation within the interlaminar region, due to the PA 66 nanofibers.

The Charpy impact strengths of the reference and PA 66 nanofiber–modified test specimens are given in Table I. The fracture energy of the reference specimens was determined as 81.45 ± 11.8 kJ/m^2. It was observed that the addition of PA 66 nanofibers within the composite's interlaminar region improved the impact fracture energy. The fracture energy values were determined as 87.19 ± 15.0 kJ/m^2 and 96.13 ± 6.9 kJ/m^2 for PA 66 nanofiber–modified composites with 0.525 g/m^2 and 1.05 g/m^2 AWD values, respectively. This corresponds to about 7% and 18% improvement in fracture energy for 0.525 and 1.05 AWD, respectively, as compared to those for composites without nanofibers. The improved impact energy can be explained by analyzing the SEM images of the fracture surfaces of the reference and PA 66 nanofiber interleaved specimens. As seen in Figure 13(a), the reference specimens had a glassy and smooth fracture surface and showed no sign of deformation. These are the main characteristics of poor interfacial bonding strength and impact energy. However, as seen in Figure 13(b,c), the PA 66 interleaved specimens exhibited a more complex and irregular fracture surface, which indicates a higher plastic deformation in the epoxy matrix and impact energy absorption. Also, this improvement is due to the presence of PA 66 nanofibers in the interlaminar region and their participation in resisting crack propagation at the moment of impact, improving the load-bearing capacity of the specimens and altering the failure modes during fracture. Moreover, as the AWD is increased, a relatively higher amount of energy is absorbed, which results in higher impact resistance.

Figure 14 shows the representative force-displacement curves of the reference and modified composite DCB specimens under Mode-I loading. The maximum load (F_{max}) values were determined as 14.46 ± 2.40 N, 16.42 ± 0.21 N, and 21.0 ± 1.09 N for the reference and PA 66–modified composites with 0.525 g/m^2 and 1.05 g/m^2 AWD values, respectively. The fracture behaviors of the reference and nanomodified laminates were observed to be almost similar. The maximum force values were found to be increased with the increase of nanofiber AWD values. The load-displacement curves of the specimens were jagged, which

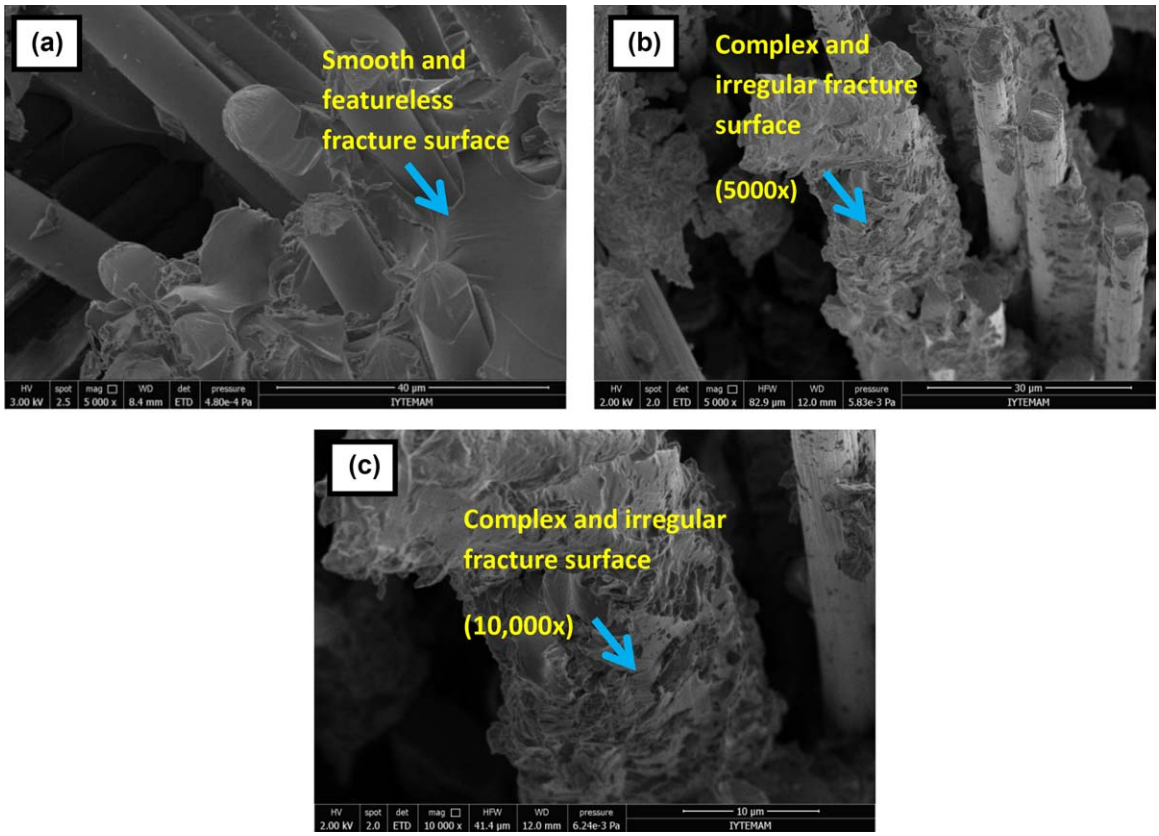

Figure 13. SEM images of fractured surface of Charpy impact specimens: (a) reference and (b,c) PA 66–modified specimens. [Color figure can be viewed at wileyonlinelibrary.com]

indicates unstable crack propagation. The crack in the reference specimens jumped more extensively during the test, although for the PA-modified specimens the crack traveled much more slowly. Therefore, the PA-modified specimens experienced a relatively more gradual load decrease, as can be seen in Figure 12. The area under the curves also represents absorbed energy during the tests. It was observed that the nanomodified specimens absorbed a greater amount of energy than did the reference specimens.

Figure 15 summarizes the initiation and propagation Mode-I interlaminar fracture toughness values for the CF/EP composites. The initiation and propagation values for the reference specimens were determined as 199 and 238 J/m^2, respectively.

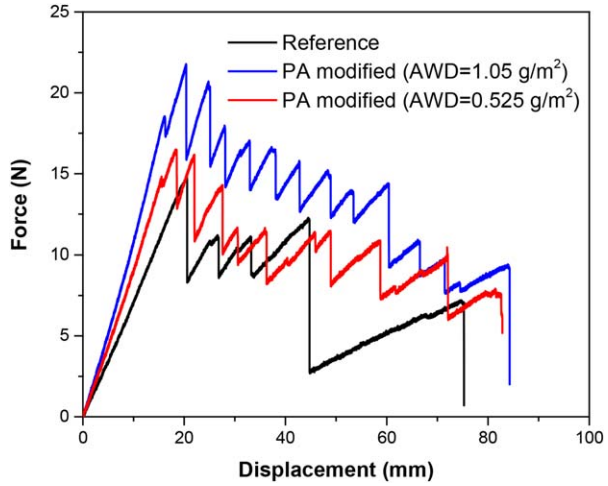

Figure 14. Representative load-displacement curves of the CF/EP DCB specimens under Mode-I loading. [Color figure can be viewed at wileyonlinelibrary.com]

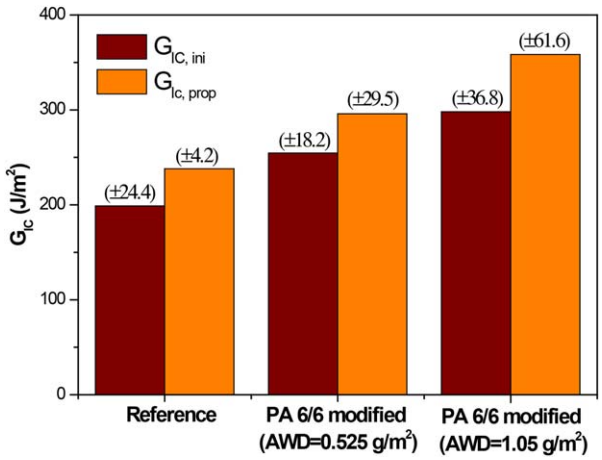

Figure 15. Initiation and propagation Mode-I interlaminar fracture toughness for the CF/EP composites. [Color figure can be viewed at wileyonlinelibrary.com]

For the composites with a 0.525 g/m^2 PA 66 nanofiber coating, the initiation and propagation Mode-I fracture toughness values were determined as 255 and 296 J/m^2, respectively. This corresponds to about 28% and 24% improvement of those values, respectively, as compared to those for the reference specimens. For the composites containing nanofibers with AWD of 1.05 g/m^2, the initiation and propagation values were found to be 298 and 358 J/m^2, which corresponds to a 50% and 51% improvement. These results clearly show that, because of the presence of nanofibers within the composites, the Mode-I fracture toughness properties are improved significantly. This is associated with the enhanced bridging mechanism promoted by nanofibers within the interlaminar region. These results also indicate that the nanofiber AWD value is a critical parameter in enhancing the cracking resistance of the composites against delamination.

The SEM images of the fracture surfaces of the Mode-I specimens with and without PA nanofibers are shown in Figure 16. The micrographs were taken from the middle of the specimens (away from the initial crack region) to interpret fracture mechanisms. As seen in Figure 16(a,c), the reference specimens exhibit smooth and featureless (indicating more brittle) failure characteristics of the composites under Mode-I loading. Mode-I fracture toughness is controlled by processes such as cohesive fracture of the matrix and fiber bridging, as stated by Greenhalgh *et al.*[1,2] Debonding of the fibers from the polymer matrix

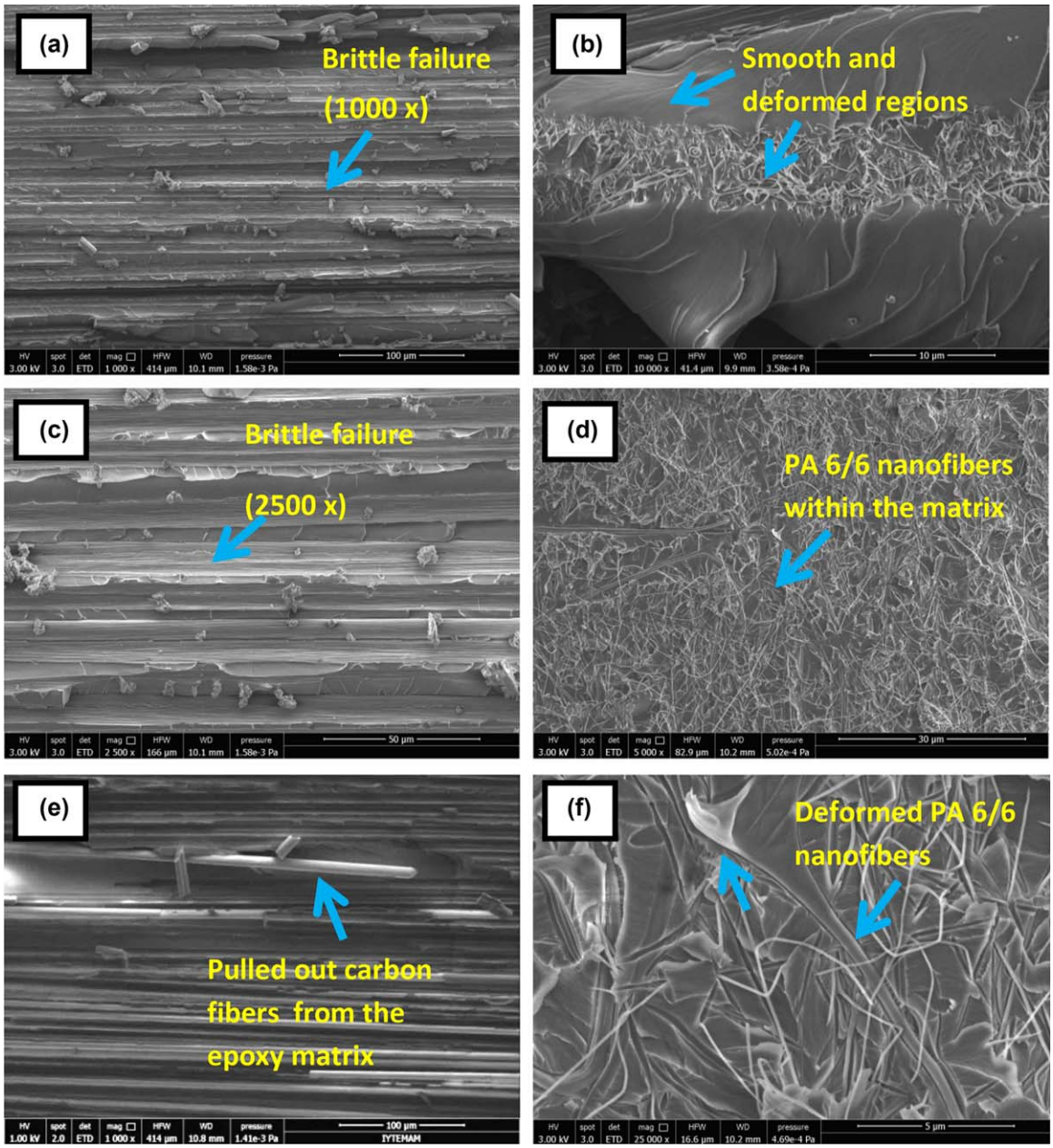

Figure 16. SEM images of fractured surface of DCB test specimens: (a,c,e) reference and (b,d,f) PA 66–modified specimens (crack propagates from left to right). [Color figure can be viewed at wileyonlinelibrary.com]

Table II. DMA Test Results of the Composites with and without PA 66 Nanofibers

Thermomechanical property	Reference specimen	PA 66 modified specimens (AWD = 0.525 g/m^2)	PA 66 modified specimens (AWD = 1.05 g/m^2)
Dynamic modulus (MPa, 25 °C)	60,751	61,196	61,308
Loss modulus (MPa, 25 °C)	1029	1010	1117
tan δ (25 °C)	0.0169	0.0173	0.0183
tan δ (peak)	0.4982	0.5249	0.5435
T_g (°C)	95.55	96.16	95.93

is visible in Figure 16(e). In the unidirectional carbon fiber composites, the main toughening mechanism is fiber bridging in the wake of the propagating crack tip. This mechanism increases the interlaminar resistance to delamination growth, especially after the crack propagates about 30–40 mm away from the crack tip. However, in this study, a limited amount of fiber bridging was observed for the reference and PA 66–modified specimens, due to the nature of the carbon fabric. It was stated in the literature that toughness values for materials that do not exhibit fiber bridging would be more accurate. Also, fiber bridging may lead to misjudging the effects of nanofiber interleaving on the fracture toughness of composites. The main fracture process observed for the reference specimens was cohesive failure of the matrix. It is also noteworthy that PA 66 nanofiber–modified specimens exhibit a combination of smooth and deformed regions (deformation of the matrix material and PA 66 nanofibers,) as seen in Figure 16(b,d). Figure 16(f) shows an example image of deformed PA 66 nanofibers within the matrix. PA 66 nylon nanofiber imprints within the matrix can also be seen in this figure. These figures support the hypothesis of more stable crack propagation in the composites with PA 66 nanofiber modification.

DMA results for the reference and PA 66 nanofiber interleaved specimens are presented in Table II. The T_g values were determined as 95.55 °C, 96.16 °C, and 96.05 °C for the reference and PA 66–modified composites with 0.525 and 1.05 g/m^2 AWD values, respectively. It was revealed that the T_g values are not affected by the incorporation of PA 66 nanofibers. This is an expected result since the fractions of the PA 66 nanofibers are relatively low. On the other hand, it was observed that the peak damping parameter (tan δ peak) of the composites is slightly increased with the incorporation of PA 66 nanofibers in the interlaminar region. Thus it was revealed that PA 66 nanofiber interleaved specimens have higher damping capacity than the reference ones. This behavior is especially important for energy absorption engineering applications.

Table III summarizes a comparison of the results obtained within the present study and those reported in the literature by other groups. As can be seen from Table III, PA 66 nanofiber interleaving is a promising technique for improving Mode-I fracture toughness of carbon fiber–epoxy composites without sacrificing the in-plane mechanical properties of those composites. Although Moroni *et al.*[31] reported a decrease in Mode-I fracture toughness values due to the presence of PA 66 nanofibers, other researchers revealed that it is possible to improve Mode-I fracture toughness values by selecting optimum electrospinning parameters, such as time or nanofiber areal weight. As a result of the work by Daelemans *et al.*[20] and Beckermann *et al.*,[32] it was shown that PA 66 nanofiber interleaving is an effective way to improve Mode-I fracture toughness when the nanofiber areal weight was between 0.5 and 9.0 g/m^2. Beckermann *et al.*[32] also revealed that there is a direct relationship between the AWD and Mode-I fracture toughness. They also showed that the effectiveness of the PA 66 nanofibers reached a maximum of Mode-I fracture toughness when the AWD was 4.5 g/m^2. In the previous studies focused on PA 66 nanofiber interleaving, the average nanofiber diameter obtained was within the range 150–200 nm. In the present work, the average diameter of the nanofibers produced was 87 nm, and the nanofiber AWD values were lower than those reported in the literature. As stated by Palazetti,[33] thinner nanofibers led to a more significant improvement in Mode-I fracture toughness. Based on these findings, it can be concluded that the present results are relevant to the findings reported in the literature. It can also be concluded that, although it is possible to obtain AWD values greater than 2 g/m^2, relatively long nanofiber coating durations may not be feasible and not applicable in industrial scales. The electrospinning parameters need to be optimized for feasible production and critical improvements in the mechanical behavior of the composites. Furthermore, recent studies also focused on the improvements of the mechanical performance of electrospun nanofibers. Xiang and Frey[35] revealed that the strength of the electrospun nylon-6 nanofibers can be increased significantly by incorporating 1 wt % carbon nanotubes (CNTs) into the fiber structure. The authors showed that the Young's modulus, tensile strength, and toughness of the PA nonwoven fiber mats increased 51, 87, and 136%, respectively, after incorporating 1 wt % CNTs into the PA nanofibers. Moreover, techniques such as thermal or solvent bonding may be tried to improve the mechanical properties of the PA nanofibers. It is also shown in Table III that the presence of PA 66 nanofibers is also effective for improving the in-plane mechanical properties, such as flexural strength, flexural modulus, and compressive strength of carbon fiber–epoxy composites. One of the key factors in this approach is the selection of polymer type for electrospinning. If the purpose of electrospun interleaving is to improve Mode-I fracture toughness together with an in-plane mechanical property such as compressive strength, PA nanofibers would be a good choice. However, as can be seen in Table III, the PA 66 nanofibers were found not to be very effective in improving the

Table III. Comparison of Results of Present Study and Other Investigations of Effect of Nanofibers on the Mechanical Properties of Composites

Reference	Average nanofiber diameter (nm)	Areal weight density (g/m^2)	Nanofiber material	Property	Improvement or reduction (%)
Present study	87 ± 22	0.525, 1.05	PA 66	Tensile strength	−9.8
				Flexural modulus	+15.6
				Flexural strength	+12.8
				Compressive strength	+15
				ILSS	+9.6
				Mode-I fracture toughness	+50
				Charpy impact strength	+18
17	150	NR[a]	PAN	Flexural strength	+55
				Flexural modulus	+20
18	300	NR	P(St-*co*-GMA)	Tensile strength	+14
20	158 ± 19	3.0	PA 66	Mode-I fracture toughness	+40
31	150 ± 20	NR	PA 66	Mode-I fracture toughness	−17
32	150–300	4.5	PA 66	Mode-I fracture toughness	+156
34	170 ± 30	NR	PA 66	Mode-I fracture toughness	+50
36	195 ± 46	1.0	PAN	Flexural strength	+54
				Flexural modulus	+21
				ILSS	+11
				Charpy impact strength	+13

[a] Not reported.

flexural strength and modulus of carbon fiber–epoxy composites as compared those obtained with PAN interleaving, as reported by Herwan *et al.*[17] and Molnar *et al.*[36] This can be explained by the fact that the elastic modulus of PAN nanofibers (7.6 GPa)[17] is higher than that of PA 66 nanofibers (0.9–1.2 GPa).[17] On the other hand, PA 66 nanofibers were more effective than PAN nanofibers in terms of absorption of impact energy. Therefore, it is very important to select the correct polymer type to obtain the desired mechanical performance.

CONCLUSIONS

In this study, electrospun PA 66 nanofibers were prepared and used as an interleaf material to improve the Mode-I fracture toughness of CF/EP composites. These nanofibers were directly collected on carbon fabrics by an electrospinning process. The electrospinning time was varied to investigate the effect of areal weight density of the nanoveils. The reference and PA 66 nanofiber interleaved specimens were manufactured by a vacuum-infusion process. A series of mechanical and thermal tests were performed to evaluate the effects of PA 66 nanofiber interleaving on the mechanical and thermal behavior of CF/EP composites. The results showed that the Mode-I fracture toughness can be improved by about 50% in both the initiation and propagation stages of the fracture using PA 66 nanofibers. The flexural modulus and strength can be increased by about 16% and 13%, respectively, with the addition of PA 66 nanofibers. ILSS values and compressive strength can be enhanced by about 10% and 15%, respectively, due to the PA 66 nanofibers. The Charpy impact energy of the composites can be increased by about 18% with the incorporation of PA 66 nanofibers with AWD values of 1.05 g/m^2. However, these nanofibers caused a decrease in tensile strength of the composites. The DMA results indicate that the T_g was not affected by the PA 66 nanofibers.

ACKNOWLEDGMENTS

The authors acknowledge KORDSA Global Inc. of Turkey for providing carbon fabrics and PA raw materials.

REFERENCES

1. Greenhalgh, E. S.; Rogers, C.; Robinson, P. *Compos. Sci. Technol.* **2009**, *69*, 2345.
2. Greenhalgh, E. S.; In Woodhead Publishing Series in Composites Science and Engineering; CRC Press: Boca Raton, FL, **2009**; pp 164–165.
3. Kuwata, M. Ph.D. Thesis, Queen Mary, University of London, **2010**.
4. Steeves, C.; Fleck, N. A. In Proceedings of the 5th Conference of Delamination and Fracture of Composites, Institute of Materials: London, UK, **1999**; Vol. *5*, pp 60–68.
5. Reeder, J. *R. J. Compos. Mater.* **1995**, *29*, 2464.
6. Jain, L. K.; Mai, Y.-W. *Compos. Sci. Technol.* **1995**, *55*, 241.
7. Tanzawa, Y.; Watanabe, N.; Ishikawa, T. *Compos. Sci. Technol.* **2001**, *61*, 1097.
8. Brandt, J.; Drechsler, K.; Arendts, F.-J. *Compos. Sci. Technol.* **1996**, *56*, 381.
9. Jain, L. K.; Mai, Y.-W. *Int. J. Fracture* **1994**, *68*, 219.

10. Ishai, O.; Rosenthal, H.; Sela, N.; Drukker, E. *Composites* **1988**, *19*, 49.
11. Sela, N.; Ishai, O.; Banks-Sills, L. *Composites* **1989**, *20*, 257.
12. Rechak, S.; Sun, C. T. *J. Reinf. Plast. Compos.* **1990**, *9*, 569.
13. Duarte, A.; Herszberg, I.; Paton, R. *Compos. Struct.* **1999**, *47*, 753.
14. Lee, S.-H.; Noguchi, H.; Kim, Y.-B.; Cheong, S.-K. *J. Compos. Mater.* **2002**, *36*, 2153.
15. Saz-Orozco, B. D.; Ray, D.; Stanley, W. F. *Polym. Compos.* **2015**, DOI: 10.1002/pc.23840.
16. Van der Heijden, S.; Daelemans, L.; De Schoenmaker, B.; De Baere, I.; Rahier, H.; Van Paepegem, W.; De Clerck, K. *Compos. Sci. Technol.* **2014**, *104*, 66.
17. Herwan, J.; Al-Bahkali, E.; Khalil, K. A.; Souli, M. *Arabian J. Chem.* **2016**, *9*, 262.
18. Bilge, K.; Venkataraman, S.; Menceloglu, Y. Z.; Papila, M. *Composites, Part A* **2014**, *58*, 73.
19. Matulevicius, J.; Kliucininkas, L.; Martuzevicius, D.; Krugly, E.; Tichonovas, M.; Baltrusaitis, J. *J. Nanomater.* **2014**, Article ID 859656.
20. Daelemans, L.; Van der Heijden, S.; De Baere, I.; Rahier, H.; Van Paepegem, W.; De Clerck, K. *Compos. Sci. Technol.* **2015**, *117*, 244.
21. Daelemans, L.; Van der Heijden, S.; De Baere, I.; Rahier, H.; Van Paepegem, W.; De Clerck, K. *Compos. Sci. Technol.* **2016**, *124*, 17.
22. Brugo, T.; Palazzetti, R. *Compos. Struct.* **2016**, *154*, 172.
23. Sanatgar, R. H.; Borhani, S.; Ravandi, S. A. H.; Gharehaghaji, A. A. *J. Appl. Polym. Sci.* **2012**, *126*, 1112.
24. Goodarz, M.; Bahrami, S. H.; Sadighi, M.; Saber-Samandari, S. *Fiber Polym.* **2017**, *18*, 322.
25. ASTM D790-10. In Annual Book of ASTM Standards; American Society for Testing and Materials: Philadelphia, PA, **1990**; p 146.
26. ASTM D 3410-87. In Annual Book of ASTM Standards; American Society for Testing and Materials: Philadelphia, PA, **1990**; pp 132–141.
27. ASTM D2344. In Annual Book of ASTM Standards; American Society for Testing and Materials: Philadelphia, PA, **2013**; pp 1–16.
28. ASTM D5528. In Annual Book of ASTM Standards; American Society for Testing and Materials: Philadelphia, PA, **2013**; pp 1–26.
29. Lee, S.-H.; Noguchi, H.; Kim, Y.-B.; Cheong, S.-K. *J. Compos Mater.* **2002**, *36*, 2169.
30. Palazzetti, R. *J. Compos. Mater.* **2015**, *49*, 3407.
31. Moroni, F.; Palazzetti, R.; Zucchelli, A.; Prondi, A. *Composites, Part B* **2013**, *55*, 635.
32. Beckermann, G. W.; Pickering, K. L. *Composites, Part A* **2015**, *72*, 11.
33. Palazzetti, R. Ph.D. Thesis, Università di Bologna, Italy, **2013**.
34. Alessi, S.; Filippo, M. D.; Dispenza, C.; Focarete, M. L.; Gualandi, C.; Palazzetti, R.; Pitarresi, G.; Zucchelli, A. *Polym. Compos.* **2015**, *36*, 1303.
35. Xiang, C.; Frey, M. W. *Materials* **2016**, *9*, 270.
36. Molnar, K.; Kostakova, E.; Meszaros, L. *eXPRESS Polym. Lett.* **2014**, *8*, 62.